

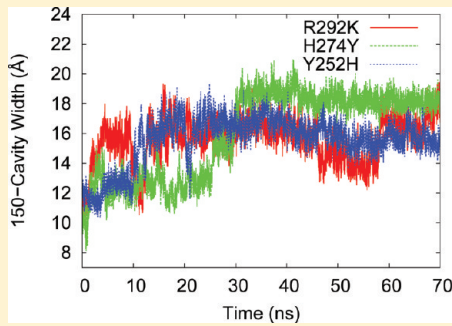
# Mutation-Induced Loop Opening and Energetics for Binding of Tamiflu to Influenza N8 Neuraminidase

Parimal Kar and Volker Knecht\*

Department of Theory and Bio-Systems, Max Planck Institute of Colloids and Interfaces, Am Mühlenberg 1, 14476 Potsdam, Germany

 Supporting Information

**ABSTRACT:** Tamiflu, also known as oseltamivir (OTV), binds to influenza A neuraminidase (H5N1) with very high affinity (0.32 nM). However, this inhibitor binds to other neuraminidases as well. In the present work, a systematic computational study is performed to investigate the mechanism underlying the binding of oseltamivir to N8 neuraminidase (NA) in “open” and “closed” conformations of the 150-loop through molecular dynamics simulations and the popular and well established molecular mechanics Poisson–Boltzmann (MM-PBSA) free energy calculation method. Whereas the closed conformation is stable for wild type N8, it transforms into the open conformation for the mutants Y252H, H274Y, and R292K, indicating that bound to oseltamivir these mutants are preferentially in the open conformation. Our calculations show that the binding of wild type oseltamivir to the closed conformation of N8 neuraminidase is energetically favored compared to the binding to the open conformation. We observe water mediated binding of oseltamivir to the N8 neuraminidase in both conformations which is not seen in the case of binding of the same drug to the H5N1 neuraminidase. The decomposition of the binding free energy reveals the mechanisms underlying the binding and changes in affinity due to mutations. Considering the mutant N8 variants in the open conformation adopted during the simulations, we observe a significant loss in the size of the total binding free energy for the N8<sub>Y252H</sub>–OTV, N8<sub>H274Y</sub>–OTV, and N8<sub>R292K</sub>–OTV complexes compared to N8<sub>WT</sub>–OTV, mainly due to the decrease in the size of the intermolecular electrostatic energy. For R292K, an unfavorable shift in the van der Waals interactions also contributes to the drug resistance. The mutations cause a significant expansion in the active site cavity, increasing its solvent accessible surface compared to the crystal structures of both the open and closed conformations. Our study underscores the need to consider dynamics in rationalizing the structure–function relationships of various antiviral inhibitor–NA complexes.



## 1. INTRODUCTION

Influenza or flu is an infectious disease caused by the influenza virus. Each year many people suffer from flu. Influenza virus can cause annual epidemics and infrequent pandemics. The virus contains a RNA (ribonucleic acid) genome, comprised of eight segments. The ability of influenza to change its antigenic structure enables it to escape the host's immune system. These changes occur in the two major surface glycoproteins: (i) hemagglutinin (HA), which binds to sialic acid (SA) receptors, and (ii) neuraminidase (NA), which cleaves SA, and facilitates the release and spread of the virus.<sup>1</sup> Vaccines have not been effective in controlling the recurring epidemics of influenza because of variation in these surface antigens.

The principal antigen on the viral surface is hemagglutinin which is the primary target for neutralizing antibodies. Hemagglutinin is responsible for viral binding to host receptors, and thus enables entry into the host cell through endocytosis and subsequent membrane fusion. HA is the most important target for developing both a drug and a vaccine against influenza. So far, 16 avian and mammalian serotypes of HA (H1–H16)<sup>2</sup> are known, but only three (H1, H2, and H3) have become adapted to the human population. Nine subtypes of

NA (N1–N9)<sup>2</sup> belonging to influenza A circulate in avian and mammalian hosts, whereas only one serotype (B) is known for influenza B. Of the nine avian influenza A NA subtypes, only N1 and N2 have been found in human viruses responsible for pandemics and recurrent annual epidemics. The N1 and N2 neuraminidases of viruses currently circulating in humans belong to two phylogenetically distinct groups.<sup>3,4</sup> Group-1 consists of N1, N4, N5, and N8, whereas the N2, N3, N6, N7, and N9 subtypes belong to group-2.<sup>3</sup> Substantial conformational differences between group-1 and group-2 neuraminidase have been observed. Group-1 NAs differ from group-2 ones by having a large cavity close to the active site cavity of the 150-loop, at residues 147–152.<sup>3</sup> The hydrophobic side chain at position 149 points away from the active site in group-1 but toward it in group-2. The active sites of all influenza neuraminidases contain three arginine residues, Arg 118, Arg 292, and Arg 371, that orient and bind to the carboxyl group of sialic acid, as well as Arg 152 that forms a hydrogen bond with

Received: March 8, 2012

Revised: May 2, 2012

Published: May 3, 2012

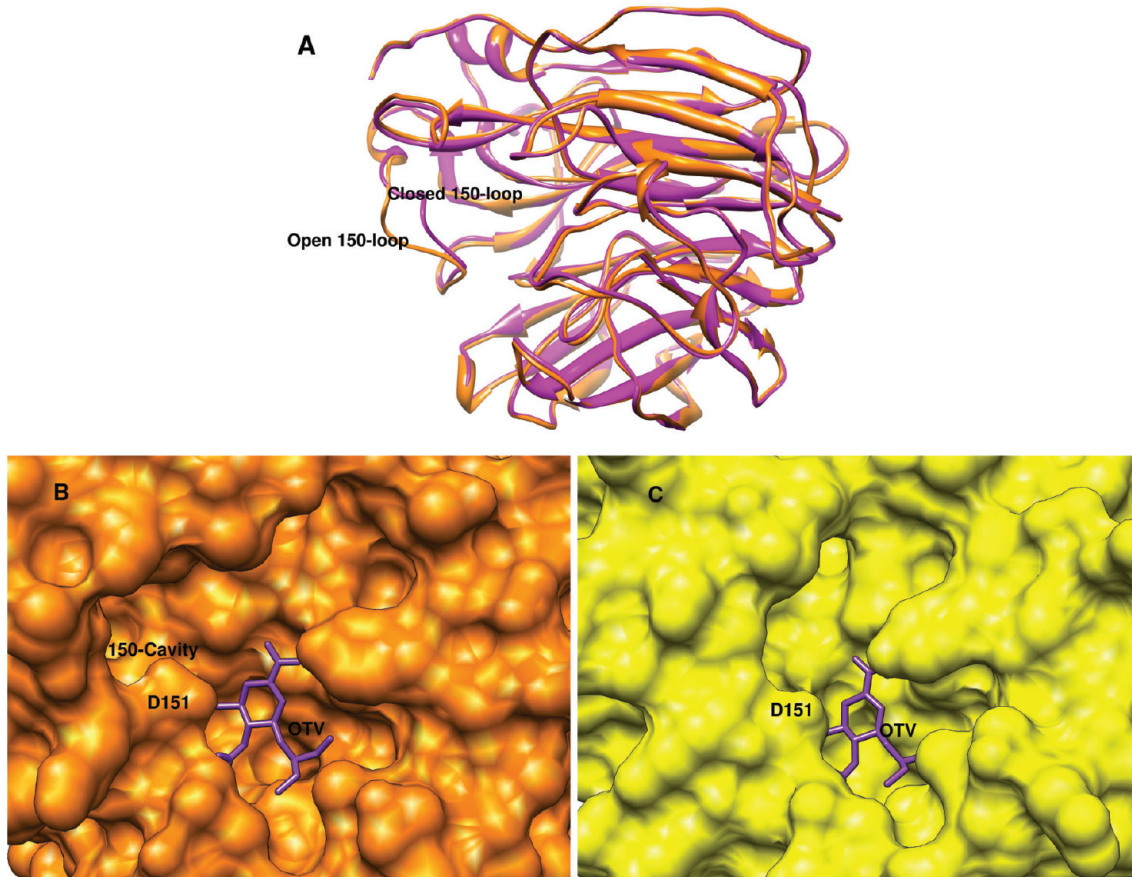


**Figure 1.** A superimposition of the open (orange) and closed (magenta) conformations of N8 neuraminidase (A) and a view of oseltamivir (purple) in the active cavity of the “open” conformation with the adjacent 150–cavity (B) and in the active cavity of the “closed” conformation of N8 neuraminidase (C). N8 is either shown in ribbon (A) or surface representation (B, C).

the acetyl amino group of the substrate and Glu 276 that forms hydrogen bonds to the 8- and 9-hydroxyl groups of the substrate.<sup>3,5</sup> NA is important during the final stage of an influenza virus infection, where it removes sialic acid from infected cell surfaces and newly formed virions, thus facilitating progeny virus release and spread of the infection to neighboring cells.

Since neuraminidase plays an essential role during the release of new virions from host cells, NA has been targeted to block its function, thereby compromising the ability of progeny virions to spread to uninfected cells. Zanamivir/ZMV (Relenza)<sup>6</sup> and oseltamivir/OTV (Tamiflu)<sup>7</sup> are two respective NA inhibitors that are frequently recommended to control the pandemics. However, the emergence of drug-resistant cases deteriorates the situation, and it is of high urgency to explore new generation anti-influenza drugs. Peramavir/PRV<sup>8</sup> is one such new generation drug which is in clinical trial now. These inhibitors are active against all influenza A and B viruses.

OTV was designed to bind against N1 and N2 neuraminidase but also binds to other NA subtypes. Russell and co-workers<sup>3</sup> have found that group-1 neuraminidases can bind oseltamivir in either the open or closed conformation of the 150-loop (see Figure 1). This depended on the time for which N8 crystals were exposed to oseltamivir solutions and the concentration of oseltamivir chosen. On the basis of these observations, a two-step process for the binding of oseltamivir to group-1 neuraminidases was proposed. According to this hypothesis, first, the inhibitor binds to the open conformation

of NA and then a slow conformational change occurs that results in the closed conformation of NA that tightly interacts with the inhibitor. The authors hypothesized that the open conformation of the loop is intrinsically lower in energy than the closed conformation, which, however, is preferred when oseltamivir is bound to N8. Taking into account this information, it should therefore be possible to design new drugs that are selective for the open 150-loop conformation and would thereby have the potential to bind more strongly than oseltamivir or zanamivir.

In this work, we have studied the binding of the inhibitor oseltamivir (OTV) to the “closed” and “open” conformations of wild type N8 neuraminidase as well as the potency of oseltamivir against mutant variants of neuraminidase. The binding of oseltamivir to the wild type and mutant variants of H5N1 was well studied. However, although the crystal structures of N8 in open and closed conformations in complex with the inhibitor OTV are available, binding affinities have not been measured experimentally. This motivated us to study these systems computationally and predict the binding free energy of OTV for the wild type and mutant N8. Oseltamivir inhibits the activity of N5 (avian H12N5), p09N1 (2009 H1N1), and p57N2 (1957 H2N2) with inhibition constants of 0.83 nM (or  $-12.5$  kcal/mol), 0.54 nM (or  $-12.8$  kcal/mol), and 0.79 nM (or  $-12.5$  kcal/mol), respectively.<sup>9</sup> This indicates that tamiflu retains a similar inhibition constant against typical group-2 and group-1 as well as atypical group-1 neuraminidases. Since N8 is a typical group-1 neuraminidase, we can

expect a similar inhibition constant for tamiflu against N8.<sup>9</sup> Oseltamivir or tamiflu is an acetamido cyclohexene that is a structural homologue of sialic acid and used to treat influenza A and B infection. It was the first orally active neuraminidase inhibitor commercially developed. The chemical structure of oseltamivir is shown in Figure 2. The information obtained

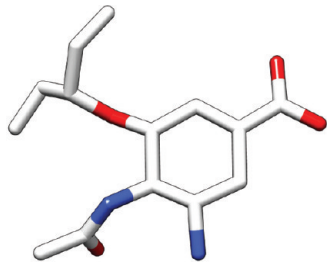


**Figure 2.** Chemical structure of oseltamivir in stick representation. Colors distinguish between carbon (white), oxygen (red), and nitrogen (blue).

from our study could be used to develop new inhibitors with improved binding properties. Using this MM/PBSA technique, we also investigate the possible role of structural water molecules mediating the N8–OTV interactions.

To understand the mechanism underlying the binding of wild-type N8 NA in “open” and “closed” conformations to OTV from an energetic point of view, we have used molecular dynamics simulations and free energy calculations to study the contributions to the binding affinities for the respective complexes. Here we follow the molecular mechanics Poisson–Boltzmann surface area (MM-PBSA)<sup>10–13</sup> scheme. In MM-PBSA methods, the binding free energy is estimated as an average of molecular mechanical energies and solvation free energies for an ensemble of configurations of a molecular complex obtained from a trajectory of a molecular dynamics simulation in explicit water. The MM-PBSA method has successfully been used to estimate the binding free energy of neuraminidase–inhibitor complexes previously.<sup>14–17</sup> The contribution from the change in entropy of the binding partners was obtained from a normal-mode analysis of the complex and the individual binding partners. Recently, Worch et al.<sup>18</sup> have modeled the interaction propensity of transmembrane domain (TMD) pairs and computed the free energy decrease for TMD dimer formation using the MM-PBSA approach. Compared to our work, the PBSA term was replaced by a multiple continua approach established to mimic biomembrane environments with the aqueous phase being modeled by water, the polar headgroup region by ethanol, and the hydrophobic core by cyclohexane.<sup>19</sup>

Recently, Wang and Zhang<sup>14</sup> have studied the selective binding of antiinfluenza drugs and their analogues to “open” and “closed” conformations of H5N1 neuraminidase. Their calculations indicate that oseltamivir prefers to bind to the closed conformation of H5N1 NA, while those having a large positively charged group generally prefer binding to the open conformation. On the other hand, our work focuses on the preferential binding of oseltamivir to “open” and “closed” conformations of N8 neuraminidase. Our calculation reveals a novel mechanism for the binding of oseltamivir to the N8 neuraminidase which differs from the mechanism for the

association of the same ligand with the H5N1 neuraminidase. We have also studied the potency of the drug against mutant variants of N8. Mutations considered in our current study are Tyr252His, His274Tyr, and Arg292Lys. These mutations are frequently observed in group-1 and group-2 neuraminidases. Our results highlight that the inherent flexibility of the 150- and 430-loops may play a role in full glycan receptor recognition, and in particular with facilitating recognition events with the distal sugar residue of different glycan receptors. It is likely that the opening and closing of the 150-loop is required for natural sialoglycan substrates to fit into the active site, given the bulky nature of these glycans.

## 2. MATERIALS AND METHODS

**2.1. Structure Generation with Periodic Boundary MD Simulations in Explicit Water.** The initial coordinates for our simulations were obtained from the X-ray crystallographic structures of the influenza A neuraminidase N8 complexed with the inhibitor oseltamivir (OTV). Recently, Russell and co-workers<sup>3</sup> have determined the X-ray crystallographic structures of the wild-type N8 complexed with the inhibitor at 2.0–2.6 Å resolution. The atomic coordinates with the Protein Data Bank accession code 2HT7 for N8<sub>open</sub>–OTV and 2HT8 for N8<sub>closed</sub>–OTV were used for our current study. However, the X-ray crystallographic structures of the mutant variants of N8 are not determined yet. Thus, the Y252H, H274Y, and R292K mutations were performed manually. Crystal waters present in 2HT8 are kept in our initial model.

The proteins were described using the Amber ff03 force field.<sup>20</sup> The ligands were assigned generalized Amber force field (GAFF)<sup>21</sup> atom types and AM1-BCC<sup>22</sup> atomic charges obtained by adding the bond charge correction (BCC) to a semiempirical quantum calculation of molecular electronic structure according to the Austin Model 1 (AM1) population atomic charge,<sup>23</sup> calculated with the antechamber<sup>24</sup> module of the Amber<sup>25</sup> molecular dynamics software package. It has been shown by Jakalian and co-workers<sup>22</sup> that atomic charges obtained from this charge model emulate the HF/6-31G\* electrostatic potential at the surface of a molecule. Our previous studies<sup>26–28</sup> show that this charge scheme is suitable for this kind of study. In order to validate the suitability of using this charge scheme and the simulation protocol chosen, we have also studied the H5N1–OTV system and reproduced the experimental binding free energy (see Table S1, Supporting Information).

The configurations were generated via simulations of the complexes in explicit water. Each complex was solvated in TIP3P<sup>29</sup> water using a truncated octahedron periodic box, extending at least 10 Å from the complex. Nearly 8400 water molecules were added to solvate the complex, and the resulting box size was nearly 88.4 Å × 88.4 Å × 88.4 Å. An appropriate number of chloride ions were added to neutralize the charge of the system. All bond lengths involving hydrogen atoms were constrained using the SHAKE<sup>30</sup> algorithm, allowing the usage of a 2 fs time-step. The temperature was kept fixed at 300 K using a Langevin thermostat with a collision frequency of 2 ps<sup>-1</sup>. The electrostatic interactions were evaluated with the particle-mesh Ewald (PME)<sup>31</sup> scheme with a fourth-order B-spline interpolation and a tolerance of 10<sup>-5</sup> in order to treat the long-range electrostatics interactions effectively and efficiently. The nonbonded cutoff was 10 Å, and the nonbonded pair list was updated every 50 fs.

The simulations were conducted according to the following protocol: (i) The complex was first optimized by 500 steps of steepest descent followed by another 500 steps of conjugate gradient minimization, keeping all atoms of the complex restrained to their initial position with a weak harmonic restraint. (ii) After the minimization, 50 ps of constant volume MD simulation with 2 kcal·mol<sup>-1</sup> Å<sup>-2</sup> restraints on the atomic positions of the complex was performed in order to equilibrate the solvent at 300 K without undesirable drifts of the structure. (iii) Next, a 50 ps MD simulation with 2 kcal·mol<sup>-1</sup> Å<sup>-2</sup> restraints on the complex was carried out at a pressure of 1 atm to equilibrate the density. (iv) Then, the complex was equilibrated for 1 ns without restraint. After the equilibration phase, a 70 ns simulation at constant pressure was conducted and the coordinates were saved every 10 ps, resulting in 7000 configurations for each simulation. Considering the relaxation processes observed during our simulations, an extended period of 60 ns was skipped for equilibration, and only the resulting final 1000 configurations were used to estimate the binding free energy.

**2.2. MM-PBSA Calculations.** The binding affinity is determined from the free energies of the receptor/neuraminidase (P), the ligand/inhibitor (L), and the complex (PL) according to

$$\Delta G_{\text{bind}} = G_{\text{PL}} - G_{\text{P}} - G_{\text{L}} \quad (1)$$

The free energy of each species (P, L, PL) is estimated from

$$G = \langle E_{\text{MM}} \rangle + \langle G_{\text{solv}} \rangle - T \langle S_{\text{MM}} \rangle \quad (2)$$

with

$$G_{\text{solv}} = G_{\text{pol}} + G_{\text{np}} \quad (3)$$

Here,  $E_{\text{MM}}$  is the molecular mechanics gas-phase energy of the species,  $G_{\text{pol}}$  is the polar contribution to the solvation free energy of the species, estimated from the solution of the linear Poisson–Boltzmann (PB) equation,  $G_{\text{np}}$  is the nonpolar solvation free energy,  $T$  the absolute temperature of the system, and  $S_{\text{MM}}$  the entropy of the species. The gas-phase molecular mechanics energy  $E_{\text{MM}}$  can be expressed as

$$E_{\text{MM}} = E_{\text{cov}} + E_{\text{elec}} + E_{\text{vdW}} \quad (4)$$

where  $E_{\text{cov}}$ ,  $E_{\text{elec}}$ , and  $E_{\text{vdW}}$  denote the contributions from covalent, electrostatic, and van der Waals interactions, respectively. The covalent or bonded term includes terms representing bond stretching ( $E_{\text{bond}}$ ), angle vibrational ( $E_{\text{angle}}$ ), and the dihedral angle torsion energies ( $E_{\text{dihedral}}$ ) according to

$$E_{\text{cov}} = E_{\text{bond}} + E_{\text{angle}} + E_{\text{dihedral}} \quad (5)$$

The nonpolar solvation term ( $G_{\text{np}}$ ) was estimated from<sup>32</sup>

$$G_{\text{np}} = \gamma A + b \quad (6)$$

with  $\gamma = 0.00542$  kcal·mol<sup>-1</sup> Å<sup>-2</sup> and  $b = 0$ . Here,  $A$  denotes the solvent accessible surface area which was estimated with a fast linear combination of pairwise overlap (LCPO) algorithm<sup>33</sup> using a probe radius of 1.4 Å.

The values in eq 2 are obtained by averaging over an ensemble of molecular configurations taken from a molecular dynamics simulation to capture the effects of motion.

A common strategy to reduce the noise as well as the computational expense and to cancel errors in simulations is to run molecular dynamics simulations on the complex only. The averages in eq 2 are determined from an ensemble of molecular

configurations obtained from such a single trajectory of molecular dynamics simulation. In this single trajectory approach, the covalent energy ( $E_{\text{cov}}$ ) as well as the intramolecular electrostatic and van der Waals energy cancel out in the calculation of  $\Delta G_{\text{bind}}$  which can significantly reduce the noise in most cases. Nevertheless, earlier studies<sup>34,35</sup> have shown that the multitrajectory and the single trajectory method yield similar trends.

Explicit water molecules were included in our calculations in order to study their effect on the binding free energy. To this aim, explicit water molecules were considered as a part of the receptor. Thus, the binding free energy could be obtained from the following equation (eq 7), which is the standard MM-PBSA approach for including selected solvent molecules:

$$\Delta G_{\text{bind}} = \Delta G_{\text{PL+WAT}} - \Delta G_{\text{P+WAT}} - \Delta G_{\text{L}} \quad (7)$$

The MMPBSA.py.MPI script in Amber-11 was used to determine the total molecular-mechanical energy ( $E_{\text{gas}}$ ), i.e., the covalent energies ( $E_{\text{cov}}$ ) as well as the van der Waals ( $E_{\text{vdW}}$ ) and electrostatic ( $E_{\text{elec}}$ ) components. This script performs automatically all the required steps to estimate the binding free energy of protein–ligand complexes using the MM-PBSA method. The electrostatic contribution to the solvation free energy ( $G_{\text{PB}}$ ) was estimated with the Poisson–Boltzmann (PB) approach using the adaptive Poisson–Boltzmann solver (APBS).<sup>36</sup> In order to solve the PB equation, the grid spacing was set to 0.5 Å in all dimensions and the dielectric constants in the protein and in the water were set to 1 and 80, respectively. The ionic strength was chosen as 0.15 M. The ratio between the longest dimension of the rectangular finite-difference grid and that of the solute was set to 4.0. The linear PB equation was solved using a maximum of 1000 iterations.

The entropy from the vibrational degrees of freedom was calculated by normal-mode analysis (NMA) of 50 configurations using the Amber *mmpbsa\_py\_nabnmode* program. Each configuration was energy minimized with a generalized-Born solvent model (nmode\_igb=1) using a maximum of 60 000 steps and a target root-mean-square (rms) gradient of 10<sup>-4</sup> kcal mol<sup>-1</sup> Å<sup>-1</sup>.

In order to understand the inhibitor–residue interaction in more detail, the interaction energy was further decomposed into the contributions from each residue of the NA by using the theory of free energy decomposition.<sup>37</sup> The decomposition of the free energy is carried out using the less accurate but more efficient generalized Born model in order to reduce the computational cost.

### 3. RESULTS AND DISCUSSION

In order to elucidate the mechanisms underlying the preferential binding of the inhibitor OTV to the wild-type N8 neuraminidase with open and closed conformations, an energetic analysis using the MM-PBSA method was conducted. To this aim, molecular configurations obtained from MD simulations of the complexes in explicit water were used for the calculation of binding free energies.

**3.1. Structural Stability.** The production simulations of 70 ns carried out for these systems were stable on the basis of the total and potential energies of these systems (data not shown) and the root-mean-square deviation (RMSD) from the X-ray structures (see Figure 3). The average root-mean-square deviations for the wild type N8<sub>open</sub>–OTV and N8<sub>closed</sub>–OTV complexes are 1.7 (0.2) and 1.9 (0.2) Å, respectively. For both complexes, the RMSD increases during the initial 30 ns and

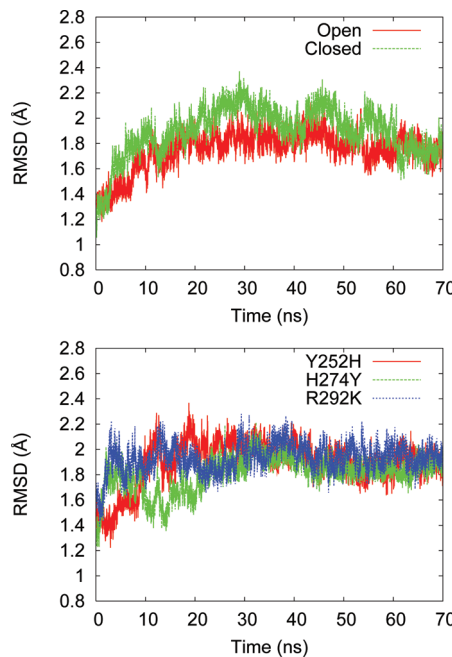


**Figure 3.** Time evolution of the root-mean-square deviations (RMSDs) of backbone atoms relative to their initial configurations for wild type N8 neuraminidase in the open and closed conformations (top) and for mutant variants in the closed conformation (bottom), in complex with oseltamivir.

then fluctuates around 1.8 Å. A similar trend was also observed for the mutant complexes. The mutations do not cause large changes in the average RMSD. We observe RMSDs of 1.9 (0.2), 1.8 (0.1), and 1.9 (0.1) Å, respectively, for the Y252H, H274Y, and R292K mutant complexes.

**Dynamics of 150-Loop.** The crystal structures of N8 neuraminidase published by Russell et al. first revealed a significant flexibility of the 150-loop.<sup>3</sup> Later, Amaro et al. studied the loop flexibility in avian influenza N1 and its implication for antiviral drug design using molecular dynamics simulations.<sup>38,39</sup> They have shown that the 150-loop is able to open into significantly wider conformations than seen in the crystal structures, suggesting that the 150-loop is even more flexible than observed in the crystal structures.<sup>38</sup> The motion of the 150-loop was found to be coupled to a motion in the neighboring 430-loop (residues 430–439), which expands the active site cavity further.<sup>38</sup> Surprisingly, the 2009 H1N1 pandemic virus (09N1) neuraminidase was crystallized without the 150-loop characteristic of group-1 NAs, indicating a high flexibility of the loop under the experimental conditions.<sup>40</sup> On the other hand, recently, Rommie et al.<sup>41</sup> have shown through molecular dynamics simulations that 09N1 neuraminidase exists in solution preferentially with an open 150-loop. Their work suggests that both N1 and N2 clinical isolates are able to adopt an open 150-loop conformation within their solution phase structural ensembles, in various relative populations, which appear to be predominantly controlled by the presence of the D147–H/R150 salt bridge.

Recently, Udommaneethanakit et al.<sup>42</sup> have studied the dynamic behavior of avian influenza A virus neuraminidase subtype HSN1 in complex with oseltamivir, zanamivir, and their phosphonate analogues. Their results indicate that neuraminidase N1 complexed with its inhibitor switches between open and closed conformations during the course of

a 20 ns molecular dynamics simulation. Their simulations show that initially closed neuraminidase N1 conformations can lose the hydrogen-bonding interaction of Asp151 with the positively charged group of inhibitors and consequently turn to the open form. Likewise, the initially open neuraminidase N1 conformations can form a hydrogen-bonding interaction between Asp151 and the cationic group of the inhibitors and consequently close—all within a single 20 ns molecular dynamics trajectory.

In this work, we have also studied the structural dynamics of the 150-loop and its implication on the binding free energy. RMSDs of the 150-loop relative to the crystal structure of wild type N8 in complex with the inhibitor obtained from our simulations are shown in Figure 4. The figure indicates that the

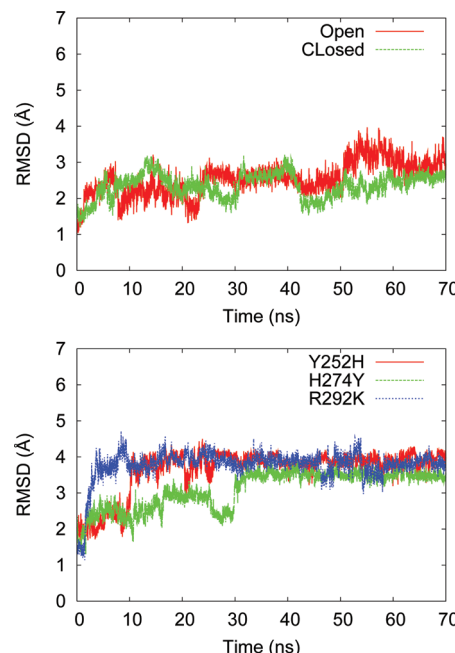


**Figure 4.** Time evolution of the root-mean-square deviations (RMSDs) of the 150-loop from crystal structures for the wild type (top) and the mutant (bottom) complexes.

150-loop for the wild type N8 in the open and closed conformations in complex with the inhibitor tamiflu remains stable on the time scale of simulations. An average root-mean-square deviation of 2.5 (0.5) and 2.6 (0.5) Å is obtained for the wild type N8 in the closed and open conformations, respectively. For all the mutant complexes, our simulations were started from the closed conformation of the 150-loop. However, the Y252H, H274Y, and R292K mutations cause a destabilization of the 150-loop indicated from a transition from the closed to the open conformation of the loop in the case of these mutant complexes (see Figure 5). These conformational changes occur after 10, 30, or 2 ns for the Y252H, H274Y, or R292K mutant, respectively, as indicated from the time evolution of the RMSD for the 150-loop shown in Figure 4. The average RMSDs for the Y252H, H274Y, and R292K mutant complexes are 3.7 (0.6), 3.5 (0.5), and 3.8 (0.4) Å, respectively.

The time evolution of the 150-loop/cavity width for each mutant is shown in Figure 6. The width refers to the distance between the alpha-carbon ( $C_\alpha$ ) of residue 431 (P431) and the closest side chain carbon of residue 149 (V149).<sup>41</sup> Figure 6 also

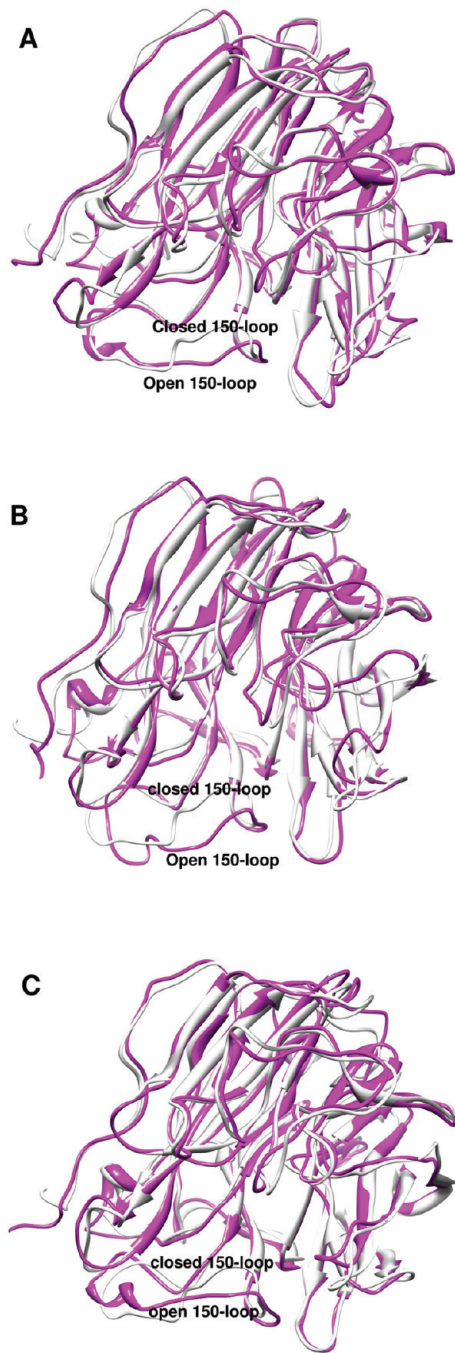


**Figure 5.** Superimposition of the wild type as well as the Y252H (A), H274Y (B), and R292K mutant N8 neuraminidase (C) in ribbon representation. The wild type and the mutants are shown in white and magenta, respectively.

indicates that a transition from the closed to the open conformation occurs after 10, 30, or 2 ns for the Y252H, H274Y, or R292K mutant, respectively. For the  $N8_{WT}^{closed}$ -OTV complex, the cavity width increases from 8 to 14 Å during the initial 30 ns and then fluctuates around 14 Å. On the other hand for  $N8_{WT}^{open}$ -OTV, the cavity width increases from 18 to 22 Å during the initial 20 ns, and then drops and fluctuates around 18 Å. During the final 10 ns of the simulations, we observe an average cavity width of 13.2 (0.9) and 17.2 Å for the wild type  $N8_{WT}^{closed}$ -OTV and  $N8_{WT}^{open}$ -OTV complexes, respectively. The cavity width for the mutant complexes resembles the cavity

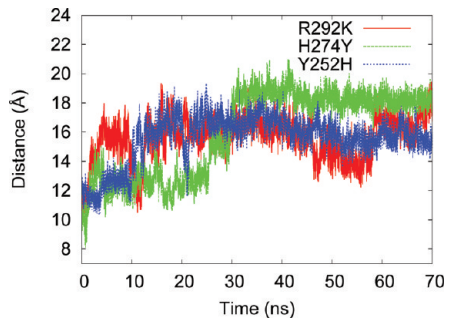


**Figure 6.** Time evolution of the 150–cavity width for wild type (top) and mutant (bottom) N8–OTV complexes. The distance between the  $C_a$  atom of residue Pro431 and the closest side chain carbon of residue Val149 is shown.

width for the wild type  $N8_{open}$ -OTV complex. The average cavity widths obtained from the final 10 ns of the corresponding simulations are 15.8 (0.7), 18.2 (0.5), and 18.2 (0.5) Å, respectively, for the Y252H, H274Y, and R292K complexes. The mutations cause a significant expansion in the active site cavity (see Figure 7), increasing its solvent accessible surface compared to the crystal structures of both the open and closed conformations (see Figure 1). A movie showing the transition from the “closed” to the “open” conformation for the R292K mutant complex is provided as Supporting Information.

To summarize, while all mutants showed a transition from the closed to the open conformation within 30 ns, the wild type N8 neuraminidase remained in the closed conformation during the whole 70 ns time scale of the simulation, indicating that the closed conformation is more stable in this case. Simulations by Rommie E. Amaro<sup>41</sup> suggest that for wild type N1, N2, and 09N1 neuraminidases the closed conformation of the 150-loop is not stable, which might indicate a difference in the behavior of these neuraminidases relative to N8 due to amino acid sequence effects. Viewing our observation that several single mutations each can significantly destabilize the closed conformation of the 150-loop for N8 variants, a difference in the behavior between N8 versus N1, N2, and 09N1 neuraminidases is plausible.

**3.2. Role of Molecular Water Structure.** Beyond the preferential binding of oseltamivir to the wild type N8 neuraminidase with closed and open conformations, we are also interested in the role of explicit water molecules in binding. In the classical MM-PBSA approach, all solvent molecules and ions are excluded. In order to capture the role of the specific water structure on the binding of oseltamivir to N8, three water molecules closest to the inhibitor are considered in our MM-PBSA calculations. The energetics of binding OTV to the wild-type  $N8_{open}$  and  $N8_{closed}$  neuraminidases with or without closest/bridge water molecules to the ligand obtained from the MM-PBSA calculations are shown in Table 1. The water mediated hydrogen bonding between the inhibitor and N8 with open and closed conformations is shown in Figure 8. We found that a water molecule forms a hydrogen-bonded bridge between oseltamivir and residue E277 for the  $N8_{open}$ -OTV complex. For the  $N8_{closed}$ -OTV complex, two water molecules are found to form a hydrogen-bonded bridge between oseltamivir and residues E277 and W178.

As shown in Table 1, the binding free energies for the  $N8_{open}$ -OTV and  $N8_{closed}$ -OTV complexes are 10.1 and 3.5 kcal/mol, respectively, when no water molecules were included in our calculations. On the contrary, the binding free energies

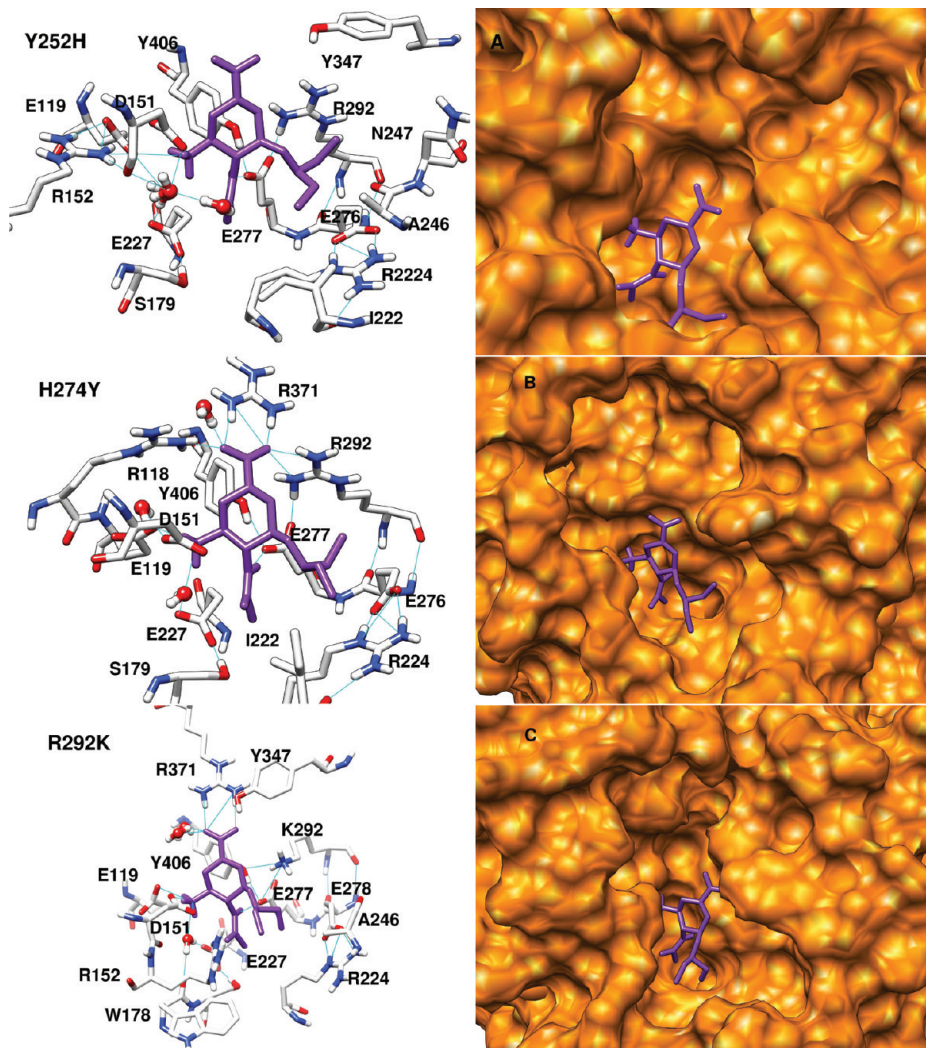


**Figure 7.** Binding mode for oseltamivir to the Y252H, H274Y, and R292K mutants and mutation-induced changes of the active cavity after 70 ns of simulation. The ligand is shown as purple sticks. On the left, the protein is depicted in stick and the water molecules in ball and stick representation. Here colors distinguish between oxygen (red), nitrogen (blue), and carbon (white). Hydrogen bonds are indicated as dotted lines. On the right, the protein is shown in surface representation.

**Table 1. Energetic Components of the Binding Free Energy for N8<sub>open</sub>-OTV and N8<sub>closed</sub>-OTV Complexes in kcal/mol<sup>a</sup>**

component	WT <sub>open</sub> <sup>f</sup>	WT <sub>closed</sub> <sup>f</sup>	WT <sub>open</sub> <sup>g</sup>	WT <sub>closed</sub> <sup>g</sup>	R292K <sub>open</sub> <sup>g</sup>	Y252H <sub>open</sub> <sup>g</sup>	H274Y <sub>open</sub> <sup>g</sup>
$\Delta E_{\text{elec}}$	-162.7(0.5)	-181.6(0.5)	-195.8(0.5)	-207.0(0.5)	-192.9(0.6)	-183.4(0.6)	-157.9(0.4)
$\Delta E_{\text{vdW}}$	-21.3(0.1)	-25.1(0.1)	-18.2(0.2)	-22.1(0.1)	-17.8(0.1)	-21.5(0.2)	-22.4(0.1)
$\Delta G_{\text{np}}$	-2.7(0.01)	-3.9(0.01)	-3.7(0.01)	-3.9(0.01)	-3.9(0.01)	-3.9(0.01)	-3.9(0.01)
$\Delta G_{\text{pol}}$	174.2(0.4)	192.4(0.4)	187.0(0.3)	191.4(0.3)	183.5(0.5)	170.3(0.5))	149.8(0.3)
$\Delta G_{\text{solv}}^b$	171.5(0.4)	188.5(0.5)	183.3(0.3)	187.5(0.4)	179.6(0.5)	166.3(0.5)	145.9(0.4)
$\Delta G_{\text{pol,elec}}^c$	11.5(0.8)	10.8(0.6)	-8.8(0.6)	-16.6(0.6)	-9.4(0.8)	-13.1(0.8)	-8.1(0.5)
$\Delta G_{\text{MM}}^d$	-184.0(0.5)	-206.7(0.5)	-213.0(0.5)	-229.1(0.5)	-210.6(0.6)	-204.9(0.7)	-180.3(0.5)
$-T\Delta S_{\text{MM}}$	22.6(2.1)	21.7(0.6)	26.1(2.1)	26.7(0.6)	20.2(1.3)	26.6(0.7)	21.9(0.9)
$\Delta G^e$	-12.5(0.5)	-18.2(0.7)	-30.7(0.6)	-41.6(0.2)	-31.0(0.3)	-38.6(0.3)	-34.4(0.2)
$\Delta G_{\text{bind}}^{\text{sim}}$	10.1(2.2)	3.5(0.9)	-4.6(2.2)	-14.9(0.7)	-10.8(1.3)	-12.0(0.8)	-12.5(0.9)

<sup>a</sup>Standard errors of the mean are provided in parentheses. <sup>b</sup> $\Delta G_{\text{solv}} = \Delta G_{\text{np}} + \Delta G_{\text{pol}}$ . <sup>c</sup> $\Delta G_{\text{pol,elec}} = \Delta G_{\text{pol}} + \Delta E_{\text{elec}}$ . <sup>d</sup> $\Delta E_{\text{MM}} = \Delta E_{\text{vdW}} + \Delta E_{\text{elec}}$ . <sup>e</sup> $\Delta G' = \Delta E_{\text{MM}} + \Delta G_{\text{solv}}$ . <sup>f</sup>No explicit water molecules considered in free energy calculation. <sup>g</sup>Three water molecules closest to the ligand considered in calculations.

become much more favorable when water molecules closest to the ligand are considered explicitly in the free energy calculations. In this case, binding free energies of -4.6 kcal/mol for the open and -14.9 kcal/mol for the closed conformations are obtained. For the N8<sub>WT</sub><sup>open</sup>-OTV complex,

an explicit treatment of water molecules closest to the ligand causes a shift in intermolecular electrostatic energy  $\Delta E_{\text{elec}}$  by -33.1 kcal/mol, while a shift of -25.4 kcal/mol is observed for the N8<sub>WT</sub><sup>closed</sup>-OTV complex. We see a decrease in the size of the van der Waals interaction energy for both complexes when

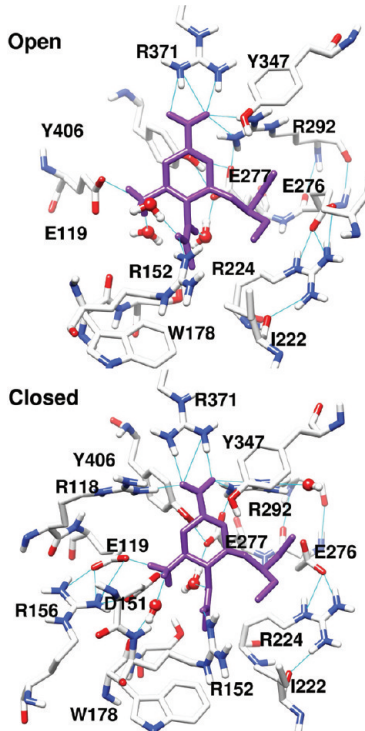


**Figure 8.** A view of the binding mode of oseltamivir (magenta) in the “open” (top) and the “closed” (bottom) conformation of N8 neuraminidase after 70 ns of MD simulation. The dotted lines represent hydrogen bonds. The representation is similar to that chosen in Figure 7.

bridge water molecules are explicitly included in our calculation. There is a shift of 3.1 and 3.0 kcal/mol, respectively, for  $N8_{WT}^{\text{open}}$ –OTV and  $N8_{WT}^{\text{closed}}$ –OTV. We find a shift in the nonpolar component of the solvation free energy by –1.0 kcal/mol for the  $N8_{WT}^{\text{open}}$ –OTV complex when water molecules are included in the calculation. In contrast, the nonpolar component of the solvation free energy for the  $N8_{WT}^{\text{closed}}$ –OTV is the same whether water molecules are included or excluded in our calculations. The polar solvation free energy is greatly affected by the bridge water molecules closest to the inhibitor in the case of  $N8_{WT}^{\text{open}}$ –OTV, where it increases by 12.8 kcal/mol. However, a mere shift of –1.0 kcal/mol in  $\Delta G_{\text{pol}}$  is observed for the  $N8_{WT}^{\text{closed}}$ –OTV complex. The total electrostatic energy  $\Delta G_{\text{pol,elec}}$  is unfavorable for both complexes when water molecules are not included in MM/PBSA. However, inclusion of water molecules in our MM/PBSA calculations leads to a favorable shift in the electrostatic energy  $\Delta G_{\text{pol,elec}}$  for both complexes. We find that  $\Delta G_{\text{pol,elec}}$  is much more favorable for the  $N8_{WT}^{\text{closed}}$ –OTV (–16.6 kcal/mol) compared to the  $N8_{WT}^{\text{open}}$ –OTV complex (–9.9 kcal/mol). Overall, these observations clearly show the significance of the molecular structure of the water close to the inhibitor in the binding of OTV to the N8 neuraminidase.

**3.3. Contribution of 150-Loop Residues to Binding Free Energy.** In order to gain insight into the effect of the structure of the 150-loop on binding at the atomic level, binding free energies were decomposed into contributions from each N8 residue. The sum of contributions from the 150-loop residues (147–152) to the binding free energy for all the complexes is shown in Table 2. Depending on whether the 150-loop adopts an open or a closed conformation, the sum of the contributions from the loop residues to the binding free energy

**Table 2. Contributions to the Binding Free Energy from 150-Loop Residues<sup>a</sup>**

$N8^{\text{open}}$	$N8^{\text{closed}}$	$Y252H_{\text{open}}$	$H274Y_{\text{open}}$	$R292K_{\text{open}}$
–3.0	–4.8	–4.8	–0.1	–2.8

<sup>a</sup>Values are given in kcal/mol.

varies. For the wild type N8 in the open or closed conformation, the sum of the total contributions to the binding free energy is –3.0 or –4.8 kcal/mol, respectively. The most significant contribution (–4.8 kcal/mol) is observed for the H274Y mutant variant of N8, the least significant contribution (–0.1 kcal/mol) is obtained for the  $N8_{R292K}$ –OTV complex, while an intermediate shift is seen for the contribution of the loop residues of –2.8 kcal/mol for the  $N8_{Y252H}$ –OTV complex.

**3.4. Binding Energetics.** The energetics for the binding of OTV to the wild type N8 in open and closed conformations and single mutant variants of N8 obtained from MM-PBSA calculations are shown in Table 1. From the table, one can see that the total binding free energies for the open and closed conformation of wild type N8 are –4.6 and –14.9 kcal/mol, respectively. This suggests that oseltamivir binds more strongly to the closed than to the open conformation of wild type N8. The total binding free energies are found to range between –14.9 and –4.6 kcal/mol. The contributions favoring binding are the van der Waals interactions between the binding partners, being in the range –17.8 to –22.4 kcal/mol, and the intermolecular electrostatic energy in the range –157.9 to –207.0 kcal/mol for all N8–inhibitor complexes. The nonpolar interactions with the solvent including the contribution from the hydrophobic effect yield contributions in the range  $-3.9 \pm 0.1$  kcal/mol for OTV complexed with the wild type and mutant variants of the  $N8^{\text{open}}$ . Association is opposed by an unfavorable desolvation of polar groups, yielding contributions between 149.8 and 191.4 kcal/mol for OTV complexed with the wild type and mutant variants of N8. For all complexes, the unfavorable desolvation of polar groups is overcompensated by favorable intermolecular electrostatic interactions. The sum of the contribution from the desolvation of polar groups and the intermolecular electrostatic interactions varies from –16.6 to –8.1 kcal/mol for the N8–inhibitor complexes.

**3.5. Mutation Induced Changes in Affinity.** To study the effects of mutations on the binding free energies, three N8 mutants in the closed conformation were considered. The mutations were Y252H, H274Y, and R292K. The mutation-induced changes in the binding free energies as well as the components of the binding free energies are summarized in Table 3. The mutations cause a shift in the binding free energies by 2.9, 2.4, and 4.1 kcal/mol, respectively, for Y252H, H274Y, and R292K. Thus, all three mutants show drug resistance against OTV. The decrease in the binding free energy due to these mutations depends on the 150-loop structure. It is seen from Figure 5 that for the Y252H, H274Y, and R292K mutants the 150-loop changes from the closed to the open conformation. These structural changes in the 150-loop are reflected in the total contribution from the loop residues (147–152) to the binding free energy. The total contributions to the binding free energy from the loop residues for all complexes are shown in Table 2. The most favorable contribution (–4.8 kcal/mol) is observed for the Y252H mutant complex, while the least favorable contribution (–0.1 kcal/mol) is observed for H274Y. For the R292K mutant, the 150-loop residues contribute –2.8 kcal/mol to the binding free

**Table 3. Free Energy Terms of N8<sub>Y252H</sub><sup>open</sup>–OTV, N8<sub>H274Y</sub><sup>open</sup>–OTV, and N8<sub>R292K</sub><sup>open</sup>–OTV Relative to the N8<sub>WT</sub><sup>closed</sup>–OTV Complex in kcal/mol<sup>a</sup>**

component	Y252H	H274Y	R292K
$\Delta\Delta E_{elec}$	23.6(0.8)	49.1(0.6)	14.1(0.8)
$\Delta\Delta E_{vdW}$	0.6(0.2)	-0.3(0.1)	4.3(0.1)
$\Delta\Delta G_{np}$	0.0(0.01)	0.0(0.01)	0.0(0.01)
$\Delta\Delta G_{pol}$	-21.1(0.6)	-41.6(0.4)	-7.9(0.6)
$\Delta\Delta G_{solv}^b$	-21.2(0.6)	-41.6(0.4)	-7.9(0.7)
$\Delta\Delta G_{pol,elec}^c$	3.5(1.0)	8.5(0.8)	7.2(1.0)
$-T\Delta\Delta S_{MM}$	-0.1(0.9)	-4.8(1.1)	6.5(1.4)
$\Delta\Delta G'^{d}$	3.0(0.3)	7.2(0.3)	10.6(0.4)
$\Delta\Delta G_{bind}^{sim}$	2.9(1.1)	2.4(1.1)	4.1(1.5)

<sup>a</sup>Standard errors of the mean are provided in parentheses. <sup>b</sup> $\Delta G_{solv} = \Delta G_{np} + \Delta G_{pol}$ . <sup>c</sup> $\Delta G_{pol,elec} = \Delta G_{pol} + \Delta E_{elec}$ . <sup>d</sup> $\Delta G' = \Delta E_{MM} + \Delta G_{solv}$ .

energy. The difference in the binding mode as well as the shape of the binding cavity for these mutant complexes are shown in Figure 7, which provides insight into the origin of mutation induced changes in the binding free energy. The change from the closed to the open conformation for the R292K mutant is shown in a movie in the Supporting Information.

**Y252H Mutant.** A shift in the binding free energy of 2.9 kcal/mol compared to the WT is detected from our calculations

for the Y252H mutant. Tables 1 and 3 show that this mutant exhibits a shift in the van der Waals energy by 0.6 kcal/mol relative to the wild type and a change in the intermolecular electrostatic energy by 23.6 kcal/mol. The nonpolar component of the solvation free energy is unaffected by the mutation. However, the Y252H mutation causes a change in the polar solvation energy which opposes binding by -21.1 kcal/mol, which is unable to compensate the unfavorable change in the intermolecular electrostatic interaction energy, leading to poor binding of the drug to the mutant compared to the wild type N8.

**H274Y Mutant.** This mutation appears to be less prone to inhibition by OTV than the wild type. The H274Y mutation causes a shift in the intermolecular electrostatic energy  $\Delta E_{elec}$  by 49.1 kcal/mol and a change in the van der Waals interaction energy  $\Delta E_{vdW}$  by -0.3 kcal/mol. The mutation does not affect the nonpolar component of the solvation free energy. However, the polar solvation free energy which disfavors the complex formation is shifted by -41.6 kcal/mol compared to the wild type. The change in the intermolecular electrostatic energy is thus not compensated by the decrease in the polar solvation free energy, leading to a poor binding compared to the wild type. The mutation causes a shift in the solute entropy by -4.8 kcal/mol. Thus, the decreased potency is driven by the intermolecular electrostatic interactions.

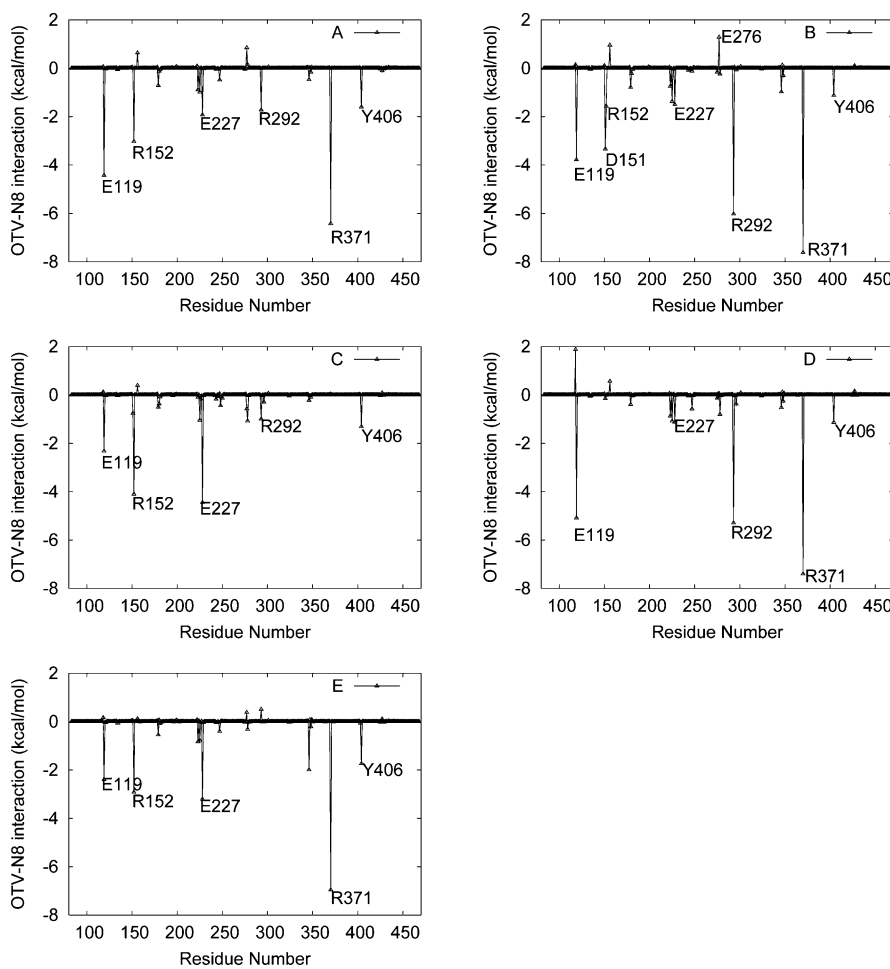


**Figure 9.** Decomposition of the binding free energy into contributions from individual residues for N8–OTV complexes. Interaction spectra for the wild type in the open (A) and closed conformation (B), as well as for the Y252H (C), H274Y (D), and R292K mutant (E) are shown. Here, the spectra for the Y252H, R292K, and R292K mutants correspond to the open conformation.

**R292K Mutant.** This mutation severely affects the binding free energy. The binding free energy is decreased by 4.1 kcal/mol compared to the wild type. Like for the Y252H mutant, drug resistance arises from the intermolecular electrostatic energy for which the R292K mutation causes a shift by 14.1 kcal/mol compared to the wild type. The van der Waals interaction energy is changed by 4.3 kcal/mol, while the nonpolar solvation free energy remains unaffected. The polar solvation free energy favors the complex formation by -7.9 kcal/mol compared to the wild type. However, this is not sufficient to compensate the shift in the intermolecular electrostatic and the van der Waals interactions energy, and, hence, is the origin of the drug resistance for this mutation.

**3.6. Interaction Energies for Selected Residues.** The inhibitor–residue interaction spectra of all N8–OTV complexes are shown in Figure 9. It is evident from the figures that the 150-loop conformation has a distinct influence on the N8–inhibitor interactions, i.e., the contributions from individual residues to the binding free energy. For the Y252H (Figure 9C), H274Y (Figure 9D), and R292K mutant complexes (Figure 9E), the spectra refer to the open conformation (Figure 9A). The wild type N8 in the closed conformation is shown in Figure 9B. Eight residues which contribute most favorably to the binding free energy of N8<sub>WT</sub><sup>closed</sup>–OTV are listed in Table 4 for all the N8–OTV complexes. This kind of decomposition of free energies helps to understand the binding mechanism as well as the origin of the change in the binding free energy due to mutations.

In the N8<sub>WT</sub><sup>open</sup>–OTV system, significant favorable contributions to the binding free energy come from residues E119 (-4.32 kcal/mol), R152 (-3.03 kcal/mol), R224 (-0.99 kcal/mol), E227 (-1.93 kcal/mol), R292 (-1.73 kcal/mol), R371 (-6.42 kcal/mol), and Y406 (-1.60 kcal/mol). In the N8<sub>WT</sub><sup>closed</sup>–OTV complex, residues E119 (-3.78 kcal/mol), D151 (-3.34 kcal/mol), R152 (-1.57 kcal/mol), R224 (-1.38 kcal/mol), E227 (-1.50 kcal/mol), R292 (-6.03 kcal/mol), Y406 (-7.62 kcal/mol), and Y406 (-1.12 kcal/mol) yield favorable contributions to the binding free energy. This helps to explain the difference in binding free energy between the open and closed conformations of N8. Residues E119, R152, E227, and Y406 contribute more favorably to the N8<sub>WT</sub><sup>closed</sup>–OTV complex formation compared to N8<sub>WT</sub><sup>open</sup>–OTV. However, OTV binds more strongly to the closed than the open conformation of N8. This is because the contributions from residues D151, R224, R292, and R371 are much more favorable in the closed than in the open conformation, leading to a significantly improved binding free energy for the closed compared to the open conformation. The contributions from D151, R292, and R371 are more favorable by -3.03, -4.3, and -1.20 kcal/mol, respectively, in the case of N8<sub>WT</sub><sup>closed</sup>–OTV compared to their contributions to N8<sub>WT</sub><sup>open</sup>–OTV.

The overall shift in the contribution from residue D151 in the closed conformation of N8 is mainly driven by the favorable shift in the intermolecular electrostatic energy by -15.98 kcal/mol compared to the contribution from the same residue in the open conformation. The configurations shown in Figure 8 suggest that the inhibitor forms a hydrogen bond with D151 in the closed conformation, while no such hydrogen bond is formed between the inhibitor and D151 in the open conformation. This is also clear from the time evolution of corresponding interatomic distances, as shown in Figure 10. Hence, we see a large shift in the intermolecular electrostatic energy. However, in the case of the N8<sub>WT</sub><sup>closed</sup>–OTV complex, the

**Table 4. Decomposition of the Binding Free Energy into Contributions from Individual Residues<sup>a</sup>**

residue	$E_{vdW}$	$E_{ele}$	$G_{pol}$	$G_{np}$	$G_{TOT}$
N8 <sub>WT</sub> <sup>open</sup> /OTV					
E119	0.59	-27.57	22.65	-0.10	-4.32
D151	-0.22	-3.0	3.23	-0.01	0.002
R152	-0.99	-6.41	4.65	-0.27	-3.03
R224	-1.37	5.86	-5.38	-0.10	-0.99
E227	-0.31	-18.48	16.89	-0.02	-1.93
R292	-0.58	-6.65	5.59	-0.90	-1.73
R371	0.42	-26.67	19.98	-0.15	-6.42
Y406	-1.78	1.83	-1.51	-0.14	-1.60
N8 <sub>WT</sub> <sup>closed</sup> /OTV					
E119	0.46	-26.12	21.92	-0.05	-3.78
D151	-0.43	-18.98	16.25	-0.18	-3.34
R152	-0.91	-1.45	0.92	-0.12	-1.57
R224	-1.69	4.03	-3.57	-0.15	-1.38
E227	-0.45	-14.28	13.23	-0.00	-1.50
R292	-0.92	-16.57	11.60	-0.14	-6.03
R371	0.74	-27.96	19.68	-0.09	-7.62
Y406	-1.35	1.65	-1.34	-0.09	-1.12
N8 <sub>Y252H</sub> <sup>open</sup> /OTV					
E119	-0.18	-18.21	16.15	-0.09	-2.33
D151	-0.63	-3.63	3.57	-0.06	-0.75
R152	-0.28	-7.06	3.41	-0.17	-4.11
R224	-1.46	2.73	-2.21	-0.10	-1.04
E227	-0.05	-28.61	24.27	-0.05	-4.45
R292	-1.37	0.65	-0.14	-0.13	-0.99
R371	-0.10	-4.44	4.59	-0.01	0.04
Y406	-1.31	2.56	-2.44	-0.12	-1.31
N8 <sub>H274Y</sub> <sup>open</sup> /OTV					
E119	0.53	-22.79	17.24	-0.07	-5.09
D151	-0.33	-3.57	3.79	-0.03	-0.15
R152	-0.12	1.35	-1.24	-0.00	-0.01
R224	-1.32	5.04	-4.72	-0.08	-1.08
E227	-0.69	-11.25	10.82	-0.01	-1.13
R292	-1.08	-15.63	11.59	-0.18	-5.29
R371	0.54	-27.63	19.79	-0.11	-7.40
Y406	-1.32	1.63	-1.35	-0.09	-1.13
N8 <sub>R292K</sub> <sup>open</sup> /OTV					
E119	0.33	-21.31	18.74	-0.16	-2.40
D151	-0.03	-0.08	0.14	0.00	0.03
R152	-0.91	-7.30	5.63	-0.34	-2.92
R224	-1.37	6.18	-5.46	-0.13	-0.78
E227	-0.43	-21.33	18.57	-0.02	-3.21
K292	-0.44	-1.16	2.20	-0.10	0.51
Y347	-0.66	-4.65	3.61	-0.29	-1.99
R371	0.54	-27.81	20.43	-0.13	-6.96
Y406	-2.14	2.32	-1.77	-0.15	-1.74

<sup>a</sup>Energetic contributions from the van der Waals ( $E_{vdW}$ ) and electrostatic interactions ( $E_{ele}$ ) as well as the polar ( $G_{pol}$ ) and nonpolar solvation free energy ( $G_{np}$ ) for N8–inhibitor complexes are listed. All values are given in kcal/mol.

contribution of the polar solvation free energy from D151 becomes more unfavorable by 13.02 kcal/mol than in the case of N8<sub>WT</sub><sup>open</sup>–OTV. Hence, the net shift in the electrostatic energy ( $E_{ele} + G_{pol}$ ) observed for this residue in N8<sub>WT</sub><sup>closed</sup>–OTV compared to N8<sub>WT</sub><sup>open</sup>–OTV is -2.96 kcal/mol. A similar trend in the contribution from R292 is observed.

**Y252H Mutant.** For this mutant, the contributions from residues R224 and Y406 do not change much. However, the

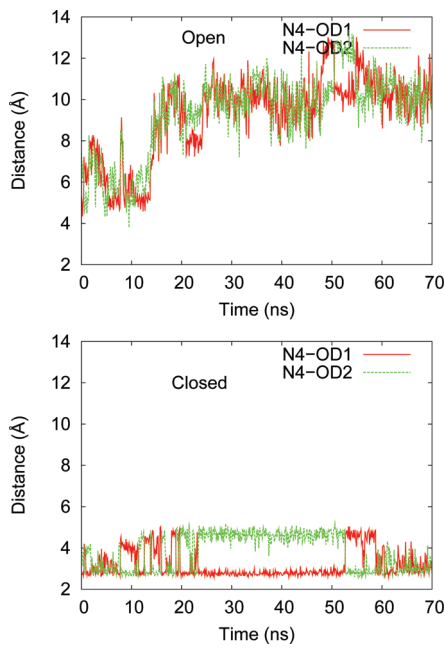


**Figure 10.** Time evolution of the distance between the side chain carbonyl oxygens (OD1 or OD2) of the residue D151 of N8 and the nitrogen (N4) atom of the ligand OTV.

sizes of the contributions from residues E119, D151, R292, and R371 are decreased significantly, leading to a significant loss in the size of the total binding free energy. The time evolutions of interatomic distances corresponding to key interactions between N8 and OTV are shown in Figure 11. The largest drop in the magnitude of the contribution is observed for residue R371 (7.66 kcal/mol) followed by R292 (5.04 kcal/mol). The contribution from E119 and D151 is decreased in size by 1.45 and 2.59 kcal/mol, respectively. The drops in the moduli of the contributions mainly arise from the decrease in the size of the intermolecular electrostatic energy ( $E_{ele}$ ).

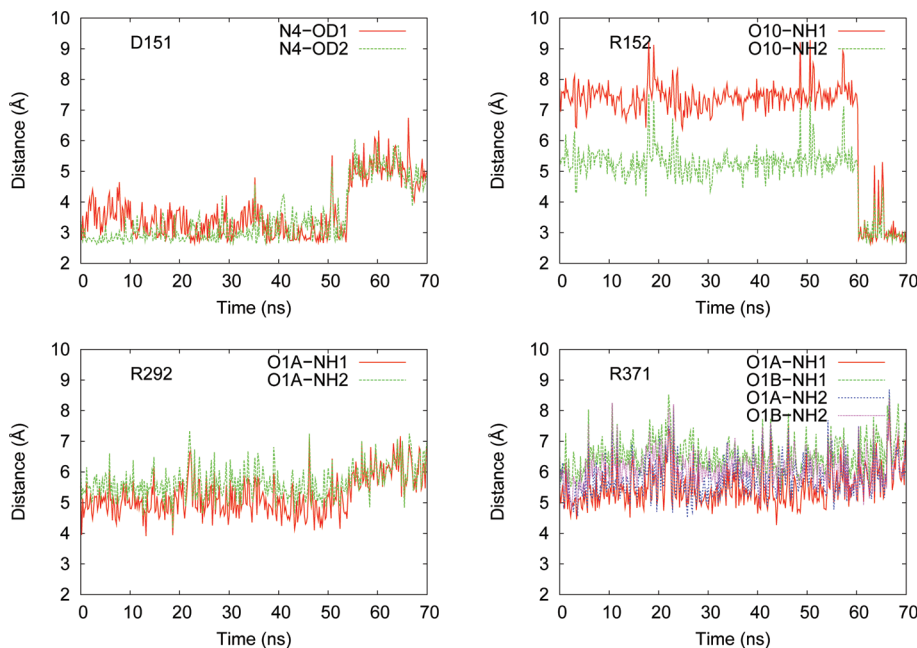


**Figure 11.** Time evolution of important interactions between OTV and N8<sub>Y252H</sub> amino acid residue side chains (D151, R152, R292, and R371).

For R292,  $E_{ele}$  is changed by 17.22 kcal/mol compared to N8<sub>WT</sub><sup>closed</sup>/OTV. However, the polar solvation free energy ( $G_{pol}$ ) becomes more favorable by -11.74 kcal/mol relative to N8<sub>WT</sub><sup>closed</sup>/OTV. The shift in  $G_{pol}$ , though, is not sufficient to counter the change in  $E_{ele}$ , leading to an unfavorable contribution of the electrostatic energy ( $E_{ele} + G_{pol}$ ) to  $G_{TOT}$ . We see hydrogen bonding between OTV and R292 in the wild type closed conformation which is lost in the Y252H mutant (see Figures 7 and 8). This is reflected in the decreased intermolecular electrostatic energy  $E_{ele}$ .

A similar trend is observed for the contribution of residue R371. For this residue,  $E_{ele}$  is decreased by 23.52 kcal/mol compared to N8<sub>WT</sub><sup>closed</sup>/OTV. However,  $G_{pol}$  is changed by -15.09 kcal/mol compared to the wild type. Hence, the net shift in the electrostatic energy ( $E_{ele} + G_{pol}$ ) is 8.43 kcal/mol, and thus unfavorable to complex formation. The shift in the intermolecular electrostatic energy correlates with the loss of hydrogen bonds between OTV and neuraminidase. For the N8<sub>WT</sub><sup>closed</sup>/OTV complex, three hydrogen bonds are formed between R371 and OTV, as shown in Figure 8. These hydrogen bonds are disrupted in the Y252H mutant, as evident from the configuration depicted in Figure 7 and the time evolution of respective interatomic distances shown in Figure 11.

**H274Y Mutant.** When His274 is replaced by Tyr, the binding free energy is decreased in size compared to the wild type. This loss in affinity is mainly due to the decrease in the magnitude of the contributions from residues D151 and R152. However, there is an increase in the size of the contributions from residues E119 (-5.09 kcal/mol). The contributions from R224, R292, and Y406 do not change much due to the mutation. The contributions from D151, R152, and R292 show shifts of 3.19, 1.56, and 0.74 kcal/mol, respectively. The increase in the size of the contributions from residue E119 is thus not enough to counter the decrease in the magnitudes of the contributions from residues D151, R152, and R292. Hence, a loss in affinity by 2.4 kcal/mol is observed for H274Y mutant. The drops in the moduli of the contributions mainly arise from

the decrease in the size of the intermolecular electrostatic energy ( $E_{\text{ele}}$ ). The intermolecular electrostatic energy is decreased in size due to the disruption of hydrogen bonds between N8 (residues D151 and R152) and oseltamivir, as evident from Figure 12.

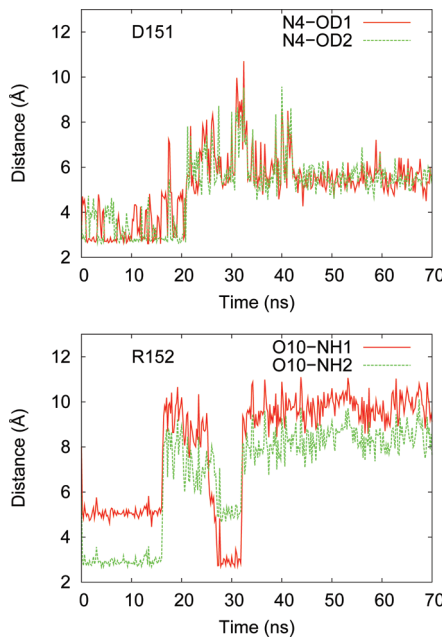


**Figure 12.** Time evolution of important interactions between  $\text{N8}_{\text{H}274\text{Y}}$  amino acid residues (D151 and R152) and the ligand oseltamivir.

**R292K Mutant.** When Arg at position 292 is replaced by Lys, the contribution to the free energy from this particular residue is decreased by 4.1 kcal/mol. This is because the R292K mutation disrupts the hydrogen bonding between the drug and the residue 292, as can be seen from Figures 8 and 7 (bottom), leading to a decrease in the size of the intermolecular electrostatic energy  $E_{\text{ele}}$  by 15.41 kcal/mol. Also, the polar solvation free energy of this residue becomes much more favorable by -9.40 kcal/mol. The magnitude of contribution from residue K292 is shifted by 6.54 kcal/mol. There is a shift in the contributions to the free energy by 3.37 or 0.6 kcal/mol from residue D151 or R224, respectively. On the other hand, residues R152 and E227 contribute more favorably to the binding free energy compared to the wild type N8 in the closed conformation. The contributions from residue R152 or E227 are shifted by -1.35 or -1.71 kcal/mol, respectively. However, the shift in the contributions from these residues is not sufficient to balance the decrease in the contributions from other residues, and hence, the drug resistance arises. The magnitudes of the contributions from residues E119, D151, R224, and R371 are decreased by 0.91, 3.09, 0.48, and 0.87 kcal/mol, respectively. The decrease in the size of the contributions from residues D151 and K292 is thus mainly responsible for the drug resistance.

#### 4. CONCLUSION

In the present work, we have studied the preferential binding of oseltamivir (tamiflu) to the open and closed conformations of N8 neuraminidase. The potency of oseltamivir against possible mutations in N8 neuraminidase was also investigated. Our calculations suggest that oseltamivir binds more strongly to N8

in the closed compared to the open conformation of the 150-loop. In a recent study, a similar selective binding of oseltamivir was observed for HSN1 neuraminidase.<sup>14</sup> In contrast to HSN1, water mediated binding of oseltamivir with the N8 neuraminidase is observed, although N1 and N8 both are group-1 neuraminidases. Whereas the closed conformation of the 150-loop was stable for the wild type for the whole 70 ns of the simulations, the mutations Y252H, H274Y, and R292K of the N8 neuraminidase induce a transition from the closed to the open conformation within 30 ns, suggesting N8 to adopt an open conformation in these cases. This structural change correlates with a decrease in binding affinity for all these mutants. The contributions to the binding free energies from the 150-loop residues are lower in the case of H274Y and R292K mutants compared to the wild type, leading to the decreased potency in the case of these mutants. For all mutants, drug resistance is found to correlate with unfavorable shifts in the intermolecular electrostatic interactions. In particular, although for the Y252H mutant the contributions to the binding free energy from the 150-loop residues are similar compared to the wild type, unfavorable shifts in intermolecular electrostatic interactions lead to drug resistance. This result is in contrast to the HSN1  $\text{N1}_{\text{Y}252\text{H}}-\text{OTV}$  complex where a gain in affinity compared to the wild type was reported. Our results emphasize the importance of dynamics in explaining the structure–function relationships of various antiviral inhibitor–NA complexes.

#### ■ ASSOCIATED CONTENT

##### Supporting Information

Table S1 showing the free energy terms for the binding of OTV to HSN1 neuraminidase and a movie showing the transition from the closed to the open conformation for the R292K mutant. This material is available free of charge via the Internet at <http://pubs.acs.org>.

#### ■ AUTHOR INFORMATION

##### Corresponding Author

\*E-mail: Volker.Knecht@mpikg.mpg.de. Phone: +49-331-5679732. Fax: +49-331-5679612.

##### Notes

The authors declare no competing financial interest.

#### ■ ACKNOWLEDGMENTS

The work was partly supported by the Federal Ministry of Education and Research (BMBF), Germany. P.K. acknowledges the financial support from the German Research Foundation (DFG) in the framework of the International Graduate Research Training Group 1524.

#### ■ REFERENCES

- (1) Murphy, B. R.; Webster, R. G. In *Fields Virology*, 3rd ed.; Fields, D. B. N., Knipe, M., Howley, P. M., Eds.; Lippincott-Raven: Philadelphia, PA, 1996; pp 1397–1445.
- (2) World Health Organization. *Bull. W. H. O.* **1980**, *58*, 585–591.
- (3) Russell, R. J.; Haire, L. F.; Stevens, D. J.; Collins, P. J.; Lin, Y. P.; Blackburn, G. M.; Hay, A. J.; Gamblin, S. J.; Skehel, J. J. *Nature* **2006**, *443*, 45–49.
- (4) Thompson, J. D.; Higgins, D. G.; Gibson, T. J. *Comput. Appl. Biosci.* **1994**, *10*, 19–29.
- (5) Clercq, E. *Nat. Rev. Drug Discovery* **2006**, *5*, 1015–1025.

- (6) von Itzstein, M.; Wu, W. Y.; Kok, G. B.; Pegg, M. S.; Dyason, J. C.; Jin, B.; van Phan, T.; Smythe, M. L.; White, H. F.; Oliver, S. W.; et al. *Nature* **1993**, *363*, 418–423.
- (7) Kim, C. U.; Lew, W.; Williams, M. A.; Liu, H.; Zhang, L.; Swaminathan, S.; Bischofberger, N.; Chen, M. S.; Mendel, D. B.; Tai, C. Y.; et al. *J. Am. Chem. Soc.* **1997**, *119*, 681–690.
- (8) Babu, Y. S.; Chand, P.; Bantia, S.; Kotian, P.; Dehghani, A.; El-Kattan, Y.; Lin, T. H.; Hutchison, T. L.; Elliott, A. J.; Parker, C. D.; et al. *J. Med. Chem.* **2000**, *43*, 3482–3486.
- (9) Vavricka, C. J.; Li, Q.; Wu, Y.; Qi, J.; Wang, M.; Liu, Y.; Gao, F.; Liu, J.; Feng, E.; He, J.; et al. *PLoS Pathog.* **2011**, *7*, e1002249.
- (10) Jayaram, B.; Sprous, D.; Young, M. A.; Beveridge, D. L. *J. Am. Chem. Soc.* **1998**, *120*, 10629–10633.
- (11) Vorobjev, Y. N.; Almagro, J. C.; Hermans, J. *Proteins* **1998**, *32*, 399–413.
- (12) Kollman, P. A.; Massova, I.; Reyes, C.; Kuhn, B.; Huo, S.; Chong, L.; Lee, M.; Lee, T.; Duan, Y.; Wang, W.; et al. *Acc. Chem. Res.* **2000**, *33*, 889–897.
- (13) Stoica, I.; Sadiq, S. K.; Coveney, P. V. *J. Am. Chem. Soc.* **2008**, *130*, 2639–2648.
- (14) Wang, P.; Zhang, J. Z. *H. J. Phys. Chem. B* **2010**, *114*, 12958–12964.
- (15) Masukawa, K. M.; Kollman, P. A.; Kuntz, I. D. *J. Med. Chem.* **2003**, *46*, 5628–5637.
- (16) Malaisree, M.; Rungrotmongkol, T.; Nunthaboot, N.; Aruksakunwong, O.; Intharathep, P.; Decha, P.; Somponpisut, P.; Hannongbua, S. *Amino Acids* **2009**, *37*, 725–732.
- (17) Nguyen, T. T.; Mai, B. K.; Li, M. S. *J. Chem. Inf. Model.* **2011**, *51*, 2266–2276.
- (18) Worch, R.; Bökel, C.; Höfinger, S.; Schwille, P.; Weidemann, T. *Proteomics* **2010**, *10*, 4196–4208.
- (19) Kar, P.; Seel, M.; Weidemann, T.; Höfinger, S. *FEBS Lett.* **2009**, *583*, 1909–1915.
- (20) Duan, Y.; Wu, C.; Chowdhury, S.; Lee, M. C.; Xiong, G.; Zhang, W.; Yang, R.; Cieplak, P.; Luo, R.; Lee, T. *J. Comput. Chem.* **2003**, *24*, 1999–2012.
- (21) Wang, J.; Wolf, R. M.; Caldwell, J. W.; Kollman, P. A.; Case, D. A. *J. Comput. Chem.* **2004**, *25*, 1157–1174.
- (22) Jakalian, A.; Jack, D. B.; Bayly, C. I. *J. Comput. Chem.* **2002**, *23*, 1623–1641.
- (23) Dewar, M. J. S.; Zoebisch, E. G.; Healy, E. F.; Stewart, J. J. P. *J. Am. Chem. Soc.* **1985**, *107*, 3902–3909.
- (24) Wang, J.; Wang, W.; Kollman, P. A.; Case, D. A. *J. Mol. Graphics Modell.* **2006**, *25*, 247–260.
- (25) Case, D. A.; Cheatham, T.; Darden, T.; Gohlke, H.; Luo, R.; Merz, K. M.; Onufriev, A., Jr.; Simmerling, C.; Wang, B.; Woods, R. J. *Comput. Chem.* **2005**, *26*, 1668–1688.
- (26) Kar, P.; Lipowsky, R.; Knecht, V. *J. Phys. Chem. B* **2011**, *115*, 7661–7669.
- (27) Kar, P.; Knecht, V. *J. Phys. Chem. B* **2012**, *116*, 2605–2614.
- (28) Kar, P.; Knecht, V. *J. Comput.-Aided Mol. Des.* **2012**, *26*, 215–232.
- (29) Jorgensen, W. L.; Chandrasekar, J.; Madura, J. D.; Impey, R.; Klein, K. *J. Chem. Phys.* **1983**, *79*, 926–935.
- (30) Ryckaert, J.-P.; Ciccotti, G.; Berendsen, H. J. C. *J. Comput. Phys.* **1977**, *23*, 327–341.
- (31) Darden, T.; York, D.; Pedersen, L. *J. Chem. Phys.* **1993**, *98*, 10089–10092.
- (32) Sitkoff, D.; Sharp, K. A.; Honig, B. *J. Phys. Chem.* **1994**, *98*, 1978–1988.
- (33) Weise, J.; Shenkin, P. S.; Still, W. C. *J. Comput. Chem.* **1999**, *20*, 217–230.
- (34) Swanson, J. M.; Henchman, R. H.; McCammon, J. A. *Biophys. J.* **2004**, *86*, 67–74.
- (35) Massova, I.; Kollman, P. A. *J. Am. Chem. Soc.* **1999**, *36*, 8133–8143.
- (36) Baker, N. A.; Sept, D.; Joseph, S.; Holst, M. J.; McCammon, J. A. *Proc. Natl. Acad. Sci. U.S.A.* **2001**, *98*, 10037–10041.
- (37) Gohlke, H.; Kiel, C.; Case, D. A. *J. Mol. Biol.* **2003**, *330*, 891–913.
- (38) Amaro, R. E.; Minh, D. D.; Cheng, L. S.; Lindstrom, W. M., Jr.; Olson, A. J.; Lin, J. H.; Li, W. W.; McCammon, J. A. *J. Am. Chem. Soc.* **2007**, *129*, 7764–7765.
- (39) Amaro, R. E.; Cheng, X.; Ivanov, I.; Xu, D.; McCammon, J. A. *J. Am. Chem. Soc.* **2009**, *131*, 4702–4709.
- (40) Li, Q.; Qi, J.; Zhang, W.; Vavricka, C. J.; Shi, Y.; Wei, J.; Feng, E.; Shen, J.; Chen, J.; Liu, D.; et al. *Nat. Struct. Mol. Biol.* **2010**, *17*, 1266–1268.
- (41) Amaro, R. E.; Swift, R. V.; Votapka, L.; Li, W. W.; Walker, R. C.; Bush, R. M. *Nat. Commun.* **2011**, *2*, 388.
- (42) Udommaneethanakit, T.; Rungrotmongkol, T.; Bren, U.; Frecer, V.; Stanislav, M. *J. Chem. Inf. Model.* **2009**, *49*, 2323–2332.